Polymer 51 (2010) 4452–4460

Contents lists available at ScienceDirect

Polymer

journal homepage: www.elsevier.com/locate/polymer

Cooperative behavior of poly(vinyl alcohol) and water as revealed by molecular dynamics simulations

Chaofu Wu

Department of Chemistry and Materials Science, Hunan University of Humanities, Science and Technology, Loudi 417000, People's Republic of China

ARTICLE INFO

Article history:
Received 26 October 2009
Received in revised form
1 June 2010
Accepted 15 July 2010
Available online 24 July 2010

Keywords:
Glass transition
Poly(vinyl alcohol)
Molecular simulations

ABSTRACT

An aqueous poly(vinyl alcohol) (PVA) model has been extensively studied by using the molecular dynamics (MD) simulation method. The employed molecular and force field models are validated against the available data in the literature. In particular, the glass transition temperature (T_g) is determined from the specific volume versus temperature, which compares well with the experimental observations. The diffusion coefficients of water (H_2O) through the PVA matrix follow the Arrhenius equations at both temperature regions separated by T_g, indicating the existence of free and bound water defined by hydrogen bonds (HBs). It has also been confirmed that HBs occur between PVA and H_2O, between PVA and PVA, between H_2O and H_2O, and all of them play the key roles in the glass transition. The local dynamics suggested by the decorrelations of various bond vectors can be well described by the Williams–Landel–Ferry (WLF) equation. This work demonstrates the cooperative behavior of PVA and H_2O which is responsible for the glass transition of the whole binary system.

1. Introduction

Structure and dynamics are closely related to the properties exhibited by polymer materials. On one hand, the glass transition temperature (T_g) can be used for characterizing the structural relaxation. On the other hand, the T_g itself, which defines the use type, is one of critical properties of polymers. Therefore, understanding the phenomenon around T_g of different polymers under various environments is of great importance academically and technically, which has been a focus of many efforts [1–12]. However, it should be noted that more deep insights are limited by the resolving power of experimental equipments. On this point, molecular simulations can be employed as important supplements since they can provide detailed information on molecular structure and intermolecular interactions. Although extensive molecular simulations have been performed to study glass transition of the pure polymers [13–15], few are devoted to the binary systems comprised of polymers and water. These model systems are of interest for the practical cases, i.e. degradation and failure of structural materials and stability of hydrogels, which deserve further investigation.

In viewpoints of molecular structure, PVA is one of most simple hydrogen bonded polymers, which can be a good model to study the complex properties of polymeric materials. About ten years ago, extensive molecular dynamics (MD) simulations on PVA–H_2O were performed by Tamai [16–22] and Muller-Plathe [23–25] and their coworkers. Several years later, Karlsson [26,27] and Chiessi [28,29] and their coworkers also carried out some MD simulations on PVA–H_2O using different molecular models. Throughout all these studies, the emphasis was put on state, structure, and dynamics of H_2O in PVA. Until the year of 2008, the effects of water on structure and dynamics of PVA chains were studied using MD methods by Bermejo and Ugarte [30]. The limited equivalence between the action of water on the polymer and the action of temperature has been proposed [31]. It has also been noted that PVA is soluble in water at high temperature but is insoluble at low temperature [17]. Judging from this phenomenon, temperature can have more impact effects on structure and properties of PVA–H_2O than does water content, which has not yet adequately studied by MD simulation methods.

In this work, MD simulations were carried out on a PVA–H_2O system with a middle water content at wide temperature range across its T_g, aiming to elucidate structure and properties of the whole system, and specially to understand glass transition in the binary system. Towards these ends, the OPLS-AA [32] and TIP4P [33] force fields were utilized to model detailed interactions for PVA and H_2O, respectively. New development of suitable force field for polyalcohols continues to attract much attention [34]. So the force field employed in this work would be validated against available data in the literature. Obtained knowledge from this study would surely contribute to develop new PVA-based

E-mail addresses: xiaowu759@hotmail.com, xiaowu759@qq.com.

0032-3861/$ – see front matter © 2010 Elsevier Ltd. All rights reserved.
doi:10.1016/j.polymer.2010.07.019

materials, such as coatings, adhesives, etc., with some improved performances.

2. Computational details

2.1. Preparation of initial model system

One single PVA chain with the degree of polymerization $n = 300$ was generated using the polymer builder in Visualizer interface of Materials Studio-4.0 [35]. The fraction of meso dyads was set as 0.5 for the atacticity. This PVA chain has two terminals, one of which is a capped hydrogen atom and the other is a methyl group. The molecular structure of PVA chain is schematically shown in Fig. 1, together with the three types of groups classified by the partial charge of atoms. The generated chain was optimized using the steepest descent (SD) and conjugate gradient (CG) methods. The optimized chain was then enclosed in a cubic box according to the Monte Carlo (MC) method developed by Theodorou and Suter [36], which is implemented in the Amorphous Cell module of Materials Studio-4.0. The periodic boundary conditions (PBC) and minimum image conventions were used to reduce the surface effects. The dimension of cubic box was defined by the target density value at 300 K, 1 g cm^3, which was about 79% of the corresponding experimental density [17], 1.27–1.31 g cm^3. By doing so, the structure was a bit easier to be equilibrated while corresponding well to the realistic system.

According to the method described above, 10 structural models were built, but only one out of them was chosen at random for the following manipulation. This structure was further optimized using SD and CG methods to remove the unreasonable close-contacts between atoms in the system. All these energy calculations were based on COMPASS force field [37] whereas the energy calculations thereafter were based on the OPLS-AA force field [32]. Note that since all the groups including alkyl and hydroxyl have been parameterized for the two force fields, both can be used to model the PVA. Here, to choose OPLS-AA instead of COMPASS is just for the technical convenience, for only the OPLS-AA is currently embraced in the much faster GROMACS-4.0.4 than the Materials Studio-4.0. However, the partial charges of atoms remained to that assigned by COMPASS force field. To choose these COMPASS charges instead of the original OPLS-AA charges is a bit arbitrary. However, their values are very similar and the COMPASS charges based on the bond-increment parameters [37] can ensure the zero charges for each charge groups, but for some groups the original OPLS-AA charges cannot.

Based on the PVA bulk structure, 200 explicit TIP4P [33] water molecules were then randomly added to the free space in the model system using the genbox routine in the GROMACS-4.0.4 [38,39]. Thus the aqueous model system contained about 21% water by weight. The so-obtained structure was optimized firstly using SD and secondly using CG, and relaxed using constant-NVE MD at first and using constant-NVT MD (at 420 K) later on. The energy minimizations (EM) were converged when the max force was smaller than 0.1 kJ mol^{-1} nm^{-1}. The MD simulations were lasted for 12 ns (1 ns = 10^{-9} s) to obtain good uniformity of water through the PVA matrix. The long-range columbic interactions were handled by the fast Particle-Mesh Ewald (PME) method. The short-range Lennard-Jones terms of the potentials were cut off at a distance of 10 Å, and the long-range correction terms were added to both energy and pressure, which was found very important to obtain desired densities and T_g. The structure of the last frame obtained from the final MD simulation is shown in Fig. 2, which is subjected to the following collecting-phase MD simulations.

2.2. Collecting-phase MD simulations

In this part, GROMACS-4.0.4 was employed for performing all the following MD simulations. Firstly, constant-NPT MD simulation was performed at 420 K and 0.1 MPa (1 MPa = 10^6 Pa) to achieve equilibrium density, which was considered as an important property to achieve dynamical properties. One structure with the density closest to the averaging one was then chosen from the last 100 ps of MD trajectory. Based on this structure and temperature, another constant-NVT MD simulation was started to achieve equilibrium energy. The system was cooled stepwise to 200 K with the temperature interval of 20 K, in which the last structure from the MD simulations at higher temperature was used as the initial structure for the MD simulations at lower temperature. Therefore, totally 12 temperatures were studied. At each temperature, a constant-NPT MD simulation of 4 ns and a constant-NVT MD simulation of 10 ns were repeated for several times. Generally, only 1–2 times were required to bring the system into equilibrium, as suggested by the temperature and energy for constant-NVT MD simulation and additional density for constant-NPT MD simulation.

The Berendsen et al. [40] methods were used for controlling the pressure and temperature at the former 500 ps, whereas the Parrinello–Rahman [41] method and the Nose–Hoover [42,43] method were used for controlling the pressure and temperature thereafter, respectively. The reasons of these choices are that the Berendsen method can quickly equilibrate temperature and pressure of the system whereas the Nose–Hoover method and Parrinello–Rahman can generate the normal ensembles. In all the MD simulations, a leap-frog algorithm with time step of 1 fs (10^{-15} s) was used for the integration of the equations of motion. None of any degrees of freedom was constrained. The MD trajectories were saved every 1000 frames (1 ps) for further analysis.

3. Results and discussion

3.1. Volumetric properties and T_g

The packing density of system is often taken as a criterion of validating the force field and molecular model used in molecular simulations. In this work, the equilibrium density was obtained by averaging over the last 3–4 ns out of the constant-NPT MD trajectory. Note that the simulated value at 300 K and 0.1 MPa for the model system is 1.20 g cm^{-3}, which is between that for pure water (about 1.00 g cm^{-3}) [17] and that for pure PVA (about 1.28 g cm^{-3}) [17]. If the macroscopic rule-of mixtures were obeyed,

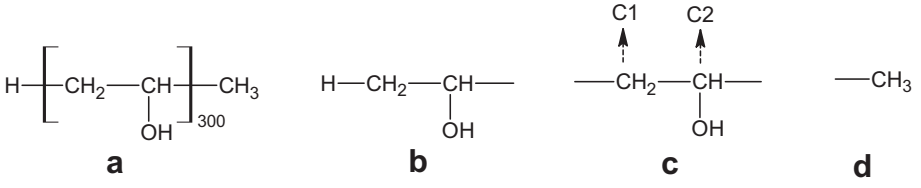

Fig. 1. Chemical structure of PVA chain (a), which is composed of three types of groups: head group (b); middle group (c); tail group (d).

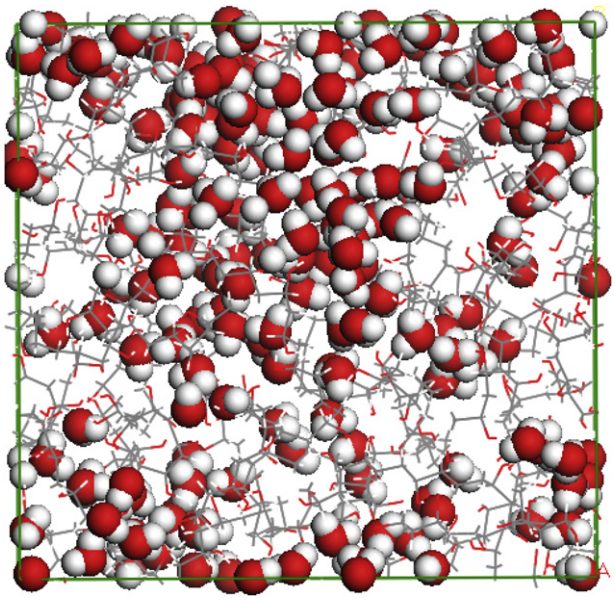

Fig. 2. Snapshot of final structure of PVA hydrogel model obtained from initial model building. The water molecules are displayed in CPK style for distinguishing from the polymer chain.

the experimental density under the same water content would be about 1.22 g cm^{-3}, which agrees very well with the simulated one.

The specific volume is plotted as a function of temperature, as shown in Fig. 3, indicating monotonic increase in the density with increasing the temperature. Furthermore, this curve shows a distinct break at around 283 K, which is identified as characteristic of vitrification. This manner in which T_g is extracted is common and empirically justified [14,15]. The simulated T_g also lies in between that for pure water (134 K) [31] and that for pure PVA (385 K) [31]. According to the sameRef. [31], variation of measured T_g with water content lower than 30 wt% (as for this work) can be modeled by the Gordon–Taylor equation:

$$\frac{1}{T_g} = \frac{w_1}{T_{g1}} + \frac{w_2}{T_{g2}} \tag{1}$$

where T_{g1}, and T_{g2} are the T_gs of pure water and pure PVA, respectively, and where w_1 and w_2 are the mass fractions of pure water and pure PVA, respectively. So the experimental T_g under the same water content to our model is about 264 K, lower by 19 K than the simulated T_g. If the fast cooling rate is taken into account, this upward discrepancy is very reasonable, which is also noted by Tamai and Tanaka [22].

Variations of specific volumes with temperatures in both regions almost approach the straight lines. By fitting the two lines by the least-squared method, the volume expansion coefficients at both temperature regions can be obtained from the slopes:

$$\alpha = \frac{1}{V_0}\left(\frac{\partial V}{\partial T}\right)_P \tag{2}$$

where α is volume expansion coefficient, V is total volume, V_0 is reference volume at 300 K, T is temperature, and P is pressure fixed. The coefficients of determination R^2 corresponding to these data at both temperature regions are beyond 0.994. The calculated volume expansion coefficient in the rubbery region is about 6.91×10^{-4} K^{-1} while that in the glass region is about 1.43×10^{-4} K^{-1}. Since the system is isotropic, the linear coefficients of thermal expansion (LCTE) in the two regions are one third of volume expansion coefficients, that is, 2.30×10^{-4} K^{-1} and 0.47×10^{-4} K^{-1}, respectively. The LCTE value above T_g is roughly consistent with the earlier range of values $(0.7–1.2) \times 10^{-4}$ K^{-1} reported for PVA [44]. The higher LCTE value with higher water content in this work can mainly result from plasticization effect of water on PVA matrix.

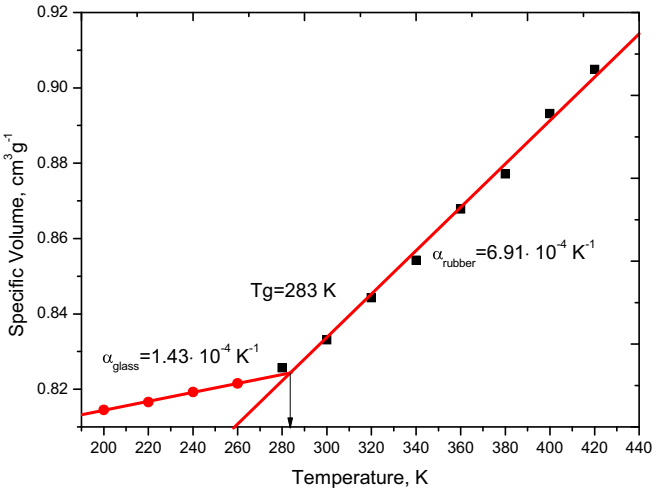

Fig. 3. Specific volume versus temperature using MD simulations for PVA–H_2O model system.

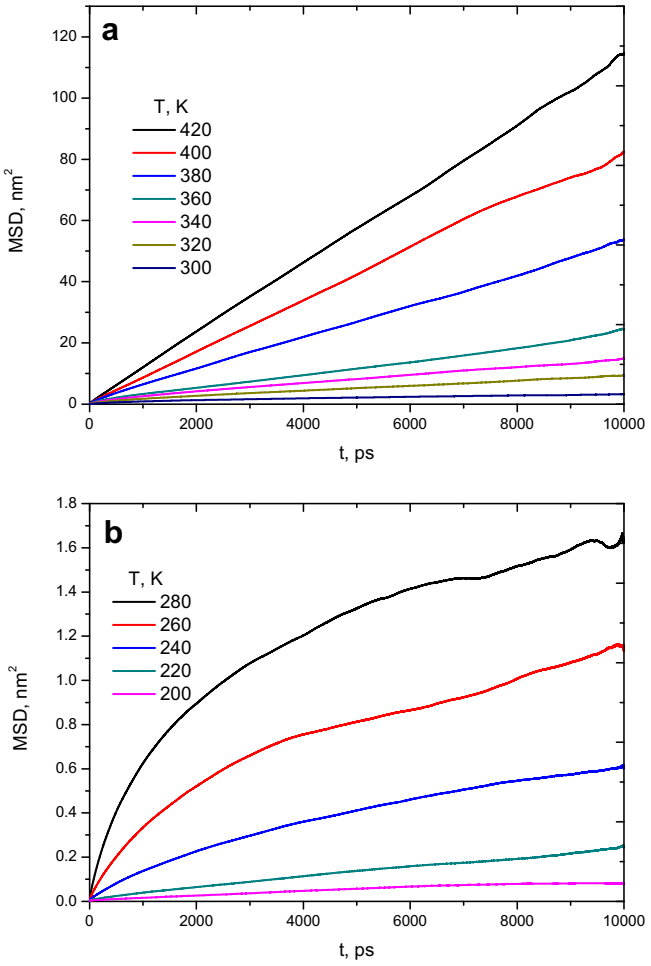

Fig. 4. MSD as functions of simulation time (t) for water in PVA at higher temperatures (a) and at lower temperatures (b).

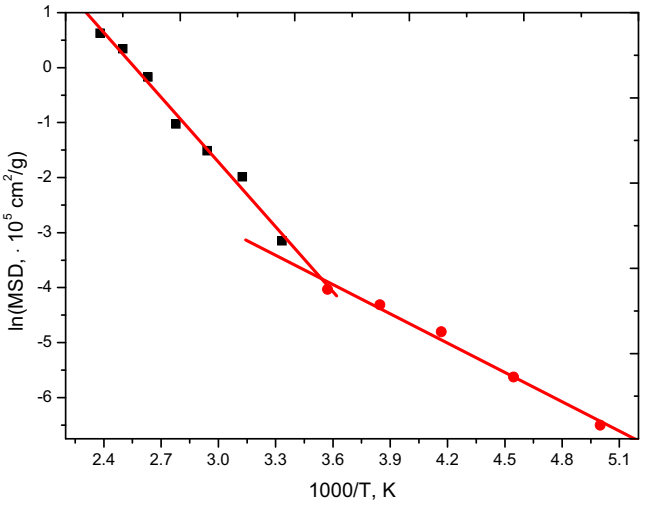

Fig. 5. Variation of diffusion coefficients with the temperature for water in PVA.

3.2. Diffusion coefficients (D) of water

Since dynamics of water depends significantly upon the surrounding environment, water can be used as the first probe to study structure and properties of the binary system. Diffusion coefficient (D) is one of good characteristic parameters of dynamics, which can be determined using the Einstein relation:

$$D = \frac{1}{6}\lim_{t\to\infty}\frac{\mathrm{d}}{\mathrm{d}t}\mathrm{MSD}(t) \tag{3}$$

where t is simulation time and MSD is mean-squared displacement. Here, MSDs with simulation time are computed from the position vectors $\vec{R}(t)$ for water molecules:

Table 1
Coordination number of water molecules to oxygen atoms of PVA at various temperatures.

T, K	r_{CD}, nm	n_{CD}
420	0.380	1.33
400	0.375	1.26
380	0.372	1.13
360	0.369	1.19
340	0.366	1.23
320	0.362	1.20
300	0.360	1.23
280	0.356	1.17
260	0.349	1.11
240	0.343	1.10
220	0.336	1.04
200	0.330	1.00

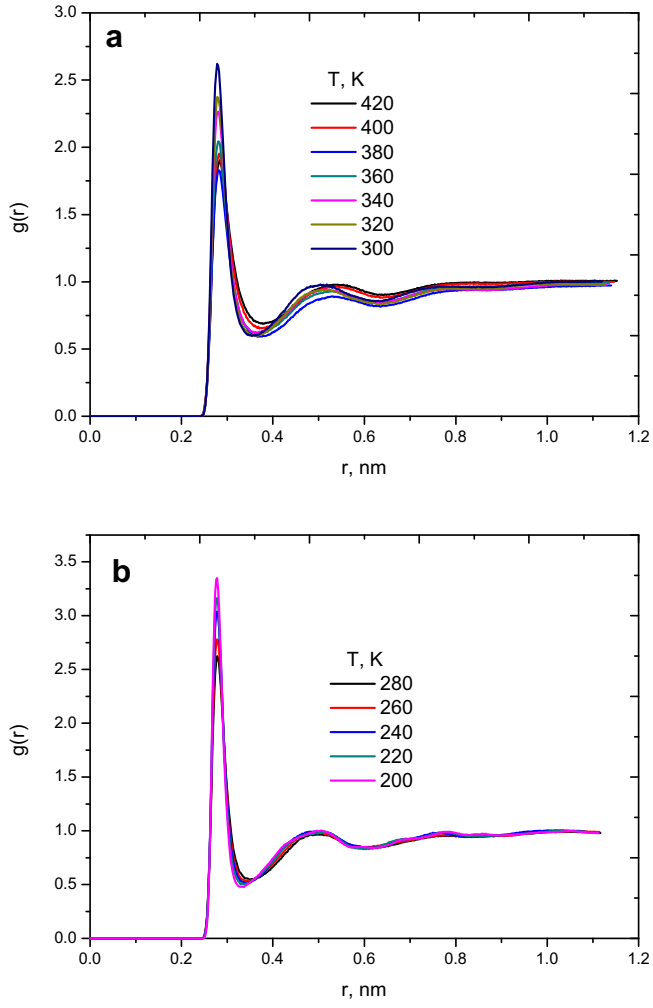

Fig. 6. RDF for O(PVA)–O(H_2O) at higher temperature region (a) and lower temperature region (b).

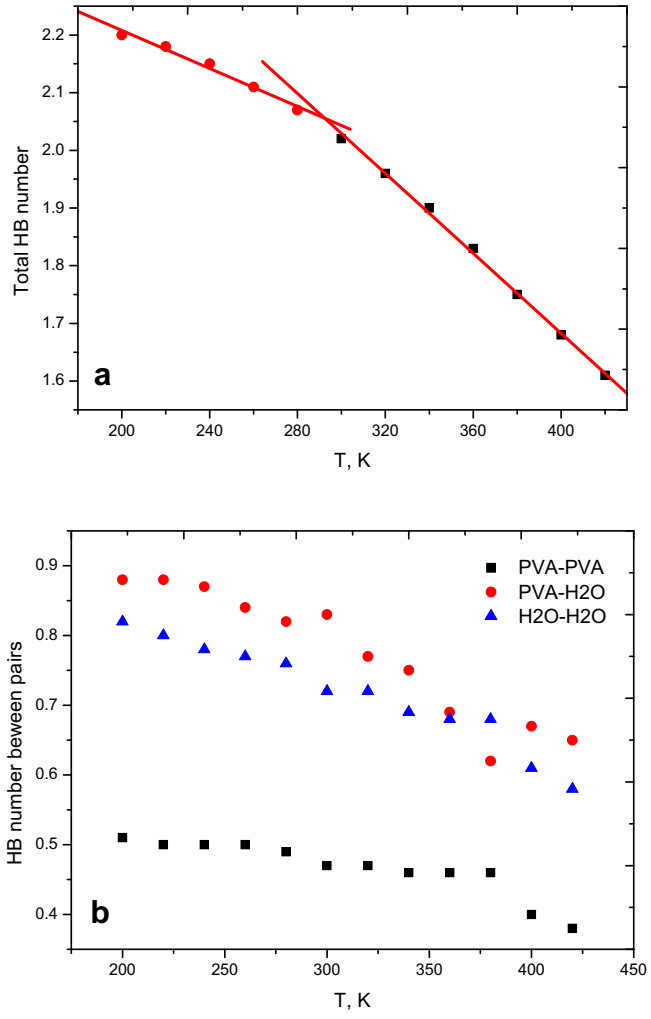

Fig. 7. Total HB number (a) and HB number between pairs (b) per hydroxyl group in the PVA–H_2O system as function of temperature.

$$\mathrm{MSD}(t) = \frac{1}{N}\sum_{i=1}^{N}\left\langle\left|\vec{R}_i(t) - \vec{R}_i(0)\right|^2\right\rangle \quad (4)$$

The broken brackets denote averaging over all choice of time origin. The results are represented collectively in Fig. 4 for various temperatures, which are divided into two sub-figures for clarity according to the two temperature regions defined by the T_g.

As expected, mobility of water within the same simulation time increases with increasing temperature. For the higher temperature region, good linearity is obtained, indicating that the diffusion approaches Fickian liquid-like behavior. However, for the lower temperature region, non-linearity up to longer time (~3 ns) is obviously seen, meaning that the diffusion is anomalous in that the water molecules spend a great deal of time sampling a local free volume in the matrix. This cage-like diffusion cannot be recognised clearly in the higher temperature region. On contrary, Karlsson et al. [26,27] reported a cage-like diffusion at above T_g for water in PVA matrix. Main reason for the difference can result from the different water content (21 wt% in this work vs. 5.2 wt% in their work), and much more water induces more lubricative effects on themselves. Moreover, in their system oxygen molecules can importantly influence the diffusion behavior of water.

The diffusion coefficients at various temperatures are calculated based on the linear parts of the MSDs. For the lower temperatures (200–280 K), the fitting is made between 3 ns and 6 ns. For the higher temperatures (300–420 K), the fitting is made between 1 ns and 8 ns. The results are shown in Fig. 5. Once again, it can be seen that the more water is the faster water moves, as suggested by the diffusion coefficients. Note that for the systems with same water content 21 wt% at 0.1 MPa, the simulated values in this work, at 300 K and 380 K, $(4.3 \pm 1.5) \times 10^{-7}$ cm^2/s and $(8.4 \pm 0.0) \times 10^{-6}$ cm^2/s, agree roughly with the values, $(6.0 \pm 2.3) \times 10^{-7}$ cm^2/s, $(2.9 \pm 0.7) \times 10^{-6}$ cm^2/s at 300 K and 375 K, respectively, reported by Muller-Plathe [45]. For the systems with different water

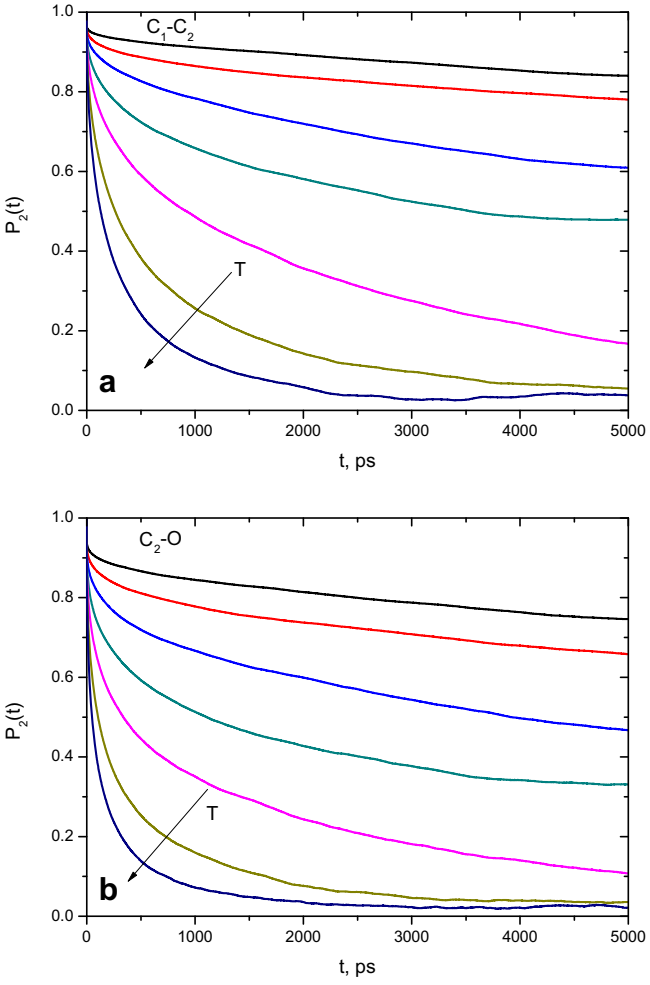

Fig. 8. Decorrelation of the C1–C2 bond vector located on the backbone (a) and the C2–O bond vector located on the aside (b) of PVA at various temperatures.

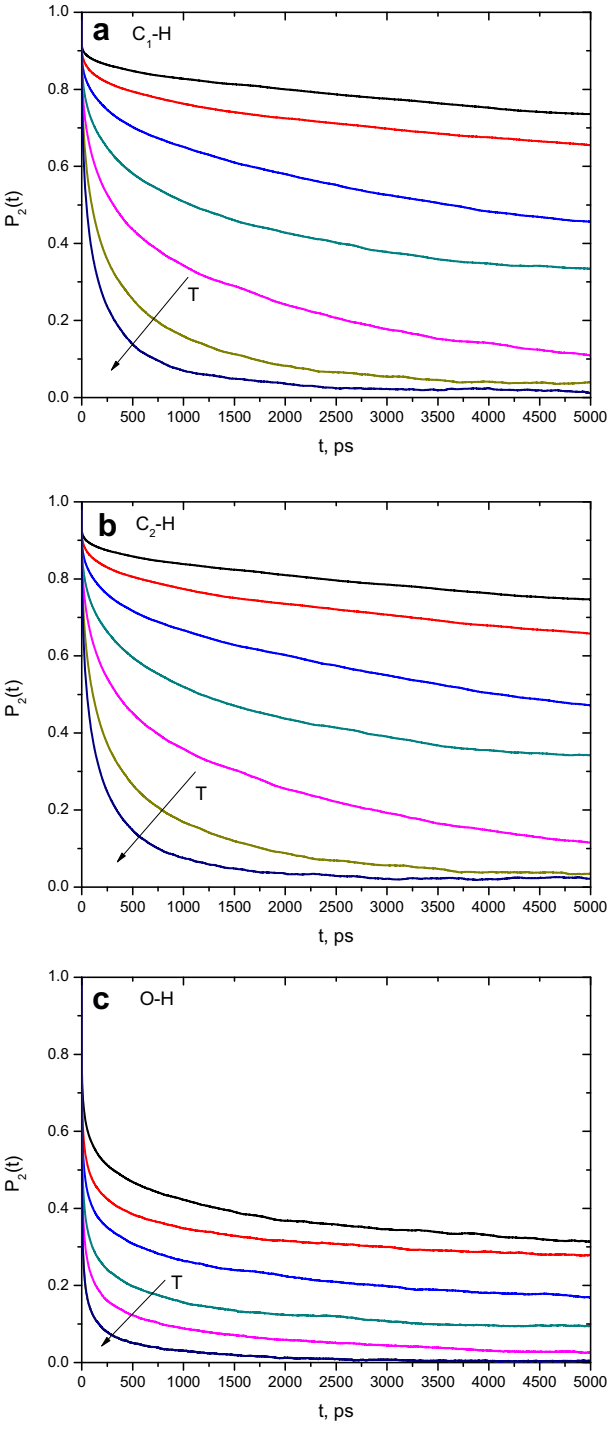

Fig. 9. Decorrelation of the C1–H bond vector (a) and C2–H bond vector (b) and O–H bond vector (c) on the PVA chain.

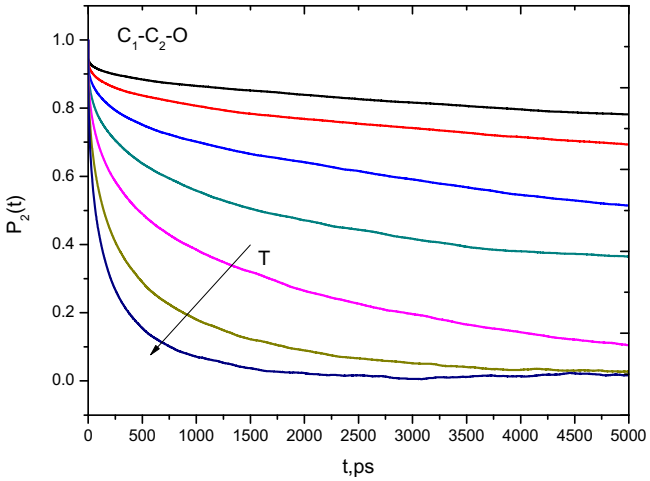

Fig. 10. Decorrelation of the C1–C2–O bond vector on the PVA chain.

contents and temperatures, similar results can also be obtained by extrapolation [25–27].

For the both temperature regions, Arrhenius relations are almost obeyed as suggested by the good linearity (the correlation coefficients R^2 are both over 0.98), as shown in Fig. 5. The straight lines in Fig. 5 are obtained by fitting to the following equation:

$$\ln D = \ln D_0 + \left(\frac{-E_D}{1000R}\right)\cdot\frac{1000}{T} \tag{5}$$

where R is general gas constant and E_D is called activation energy. The calculated values of E_D are about 3.58 kcal/mol (1 kcal = 4.18 J) and 7.75 kcal/mol for higher temperature region and lower temperature region, respectively. These values have the same order of magnitude as the reported ones, 4.5 ± 0.5 kcal/mol obtained using MD simulations [28] and 4.0 ± 0.6 kcal/mol obtained in the QENS study [28]. The simulated activation energy at lower temperatures is lower by 4.17 kcal/mol than that at higher temperatures, which is on the order of the energy for hydrogen-bonding between PVA and H_2O, that is, 4.71–5.15 kcal/mol [17].

Here, for the first time, we report there is a break in the plot of ln (D)–1000/T for the PVA–H_2O binary system. Similar phenomena have also been discovered for the polar polymer–water systems, water–epoxy system [46] and water–polyacrylate latex film [47]. These phenomena can be explained by the different desorption activation energies of free water and bound water in the polymer matrixes. Just as the name implies, the two types of water are defined according to whether they bound to the polymers through the hydrogen-bonding (HB) interactions [8]. In the lower temperature region, only free water can be desorbed whereas in the higher temperature region, both free water and bound water can be desorbed. The two types of water correspond to two different desorption activation energies. And it is obvious that the bound water has higher desorption activation energy than the free water.

Interestingly, the slope changes of Arrhenius plots have been also found for the apolar polymer systems, PE–CO_2 [48] and PS–CO_2 and PS–C_3H_8 [49]. Differently, activation energy at lower temperature region is higher than that at higher temperature region. Since no HBs are presented, it corresponds to a different mechanism. It is worthy of pointing out that, for the non-HB polymeric system [48], the difference in activation energy between the two temperature regions is much smaller than those for the HB polymeric systems [46,47]. This comparison illustrates the importance of HB interactions in the desorption process.

Finally, the break in the ln(D)–1000/T plot is found to occur at around T_g. This phenomenon can also be explained as the abrupt increase of HB interactions at T_g from the higher temperature, which is discussed below.

3.3. Hydrogen bonds (HBs) interactions

3.3.1. Radial distribution functions

RDF provides a first insight into the HB interactions, which can be calculated using the following formula

$$g_{AB}(r) = \frac{\langle \rho_B(r) \rangle}{\rho_B} \tag{6}$$

The numerator in this formula is particle density of type B at a distance around A, which can be computed according to the following formula:

$$\langle \rho_B(r) \rangle = \frac{1}{N_A}\sum_{i\in A}^{N_A}\sum_{i\in B}^{N_B}\frac{\delta(r_{ij}-r)}{4\pi r^2} \tag{7}$$

in which delta function is either 1 or 0, depending on if the distance difference is within the ranges considered. The denominator in formula 6 is particle density of type B averaged over all spheres, which can be calculated as the number of particle B per unit volume:

$$\rho_B = \frac{N_B}{V} \tag{8}$$

The intermolecular RDFs of O_p–O_w are computed for oxygen of PVA and oxygen of H_2O at various temperatures, as shown in Fig. 6. The shape of RDFs is very similar to that obtained by other authors [16,17,28–30]: one sharp peak at about 0.28 nm and one broad peak at about 0.49 nm. When the ethanol molecules were added [23], however, more peaks would be present, resulting from the additional complex interactions. The sharp peak marks the occurrence of HBs between PVA and H_2O, which defines the first hydration shell on PVA oxygen. Likewise, the broad peak is attributed to the presence of a second hydration shell on PVA oxygen. No obvious peaks are seen at the distance longer than 0.8 nm, indicating the amorphous feature of the system.

Table 2
Correlation time of various bond vectors on the PVA chains.

T, K	Correlation time, ps					
	C1–H	C2–H	O–H	C1–C2	C2–O	C1–C2–O
420	312.8	323.7	62.4	522.5	321.5	288.8
400	675.7	704.4	136.8	1078.8	660.8	706.7
380	2474.5	2757.4	935.1	3481.2	2456.2	2345.0
360	27,272.5	22,767.6	2084.3	38,184.9	18,296.2	20,378.1
340	60,011.9	63,588	62,605.7	75,915.3	52,325	76,584.9
320	4,186,390	2,076,030	5,123,540	4,100,270	1,185,300	1,429,390
300	10,553,400	7,718,760	698,811	3,396,860	2,407,820	5,642,190

With increasing temperature, the heights of the sharp peaks become lower and the positions of the broad peaks shift slightly towards the longer distance (the positions the broad peaks start and the sharp peaks terminate are shown as r_{CD} in Table 1). Tamai et al. [17] and Bermejo and Ugarte [30] have reported that water content has similar effect on RDFs, which demonstrates that the higher temperature has equivalent effect to the higher water content on RDFs. Shorter distance the sharp peaks locate also indicates water molecules prefer in the vicinity of hydroxyl groups than on methyl groups of PVA [30]. From this sharp peak region, the coordination number n_{CD} of water molecules to oxygen atoms of PVA can be calculated according to the following relation:

$$n_{CD}(r) = 4\pi\rho_B \int_0^{r_{CD}} g_{AB}(r) r^2 \, dr \quad (9)$$

where r_{CD} is the location of the first minimum in RDF. The values of r_{CD} and n_{CD} are shown in Table 1 for various temperatures. It can be seen that the r_{CD} has slight temperature dependence. This is also equivalent to the effect of water content on r_{CD}, as reported by Tamai et al. [16]. The n_{CD} can only be considered to be accurate within the range of 1.0–1.4, which compares well with the PVA–H_2O systems with similar temperatures and water contents [17,30]. For the PVA–H_2O systems with much higher temperatures or water contents, the n_{CD} is reasonably a bit bigger [16,17,28–30,50].

3.3.2. Number of HB using the geometric criterions

Counting the number of HB may be more direct way than the RDFs of O_w–O_p available for studying HBs. Towards this aim, the following geometric criteria are used to define an HB: (1) the distance between donor and acceptor is less than 0.35 nm and (2)

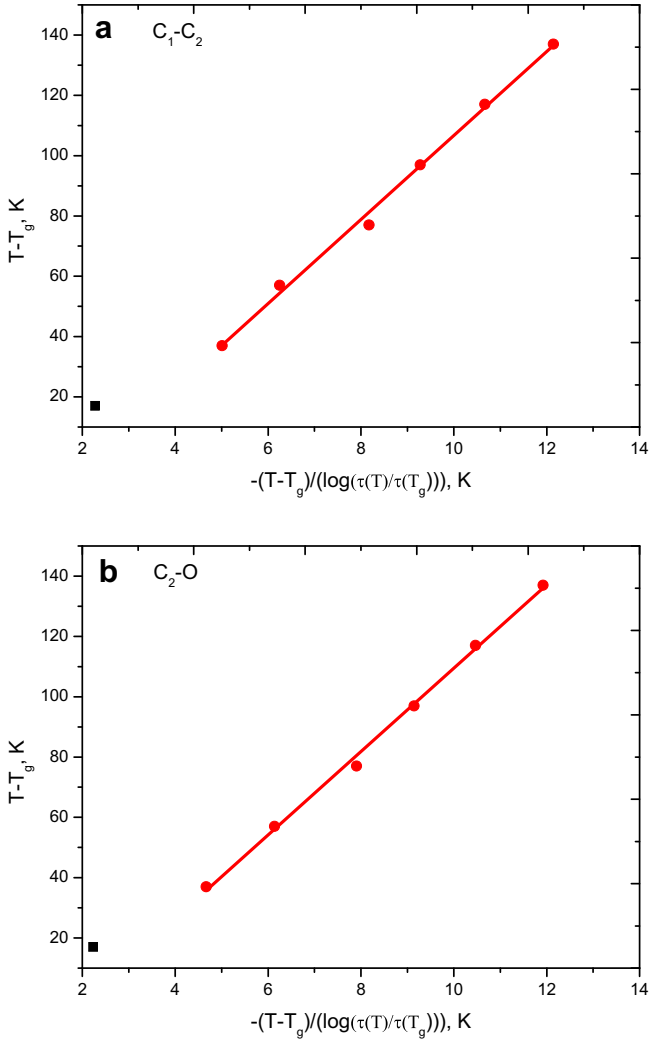

Fig. 11. WLF fit of C1–C2 bond vector (a) and C2–O bond vector (b) on the PVA chain.

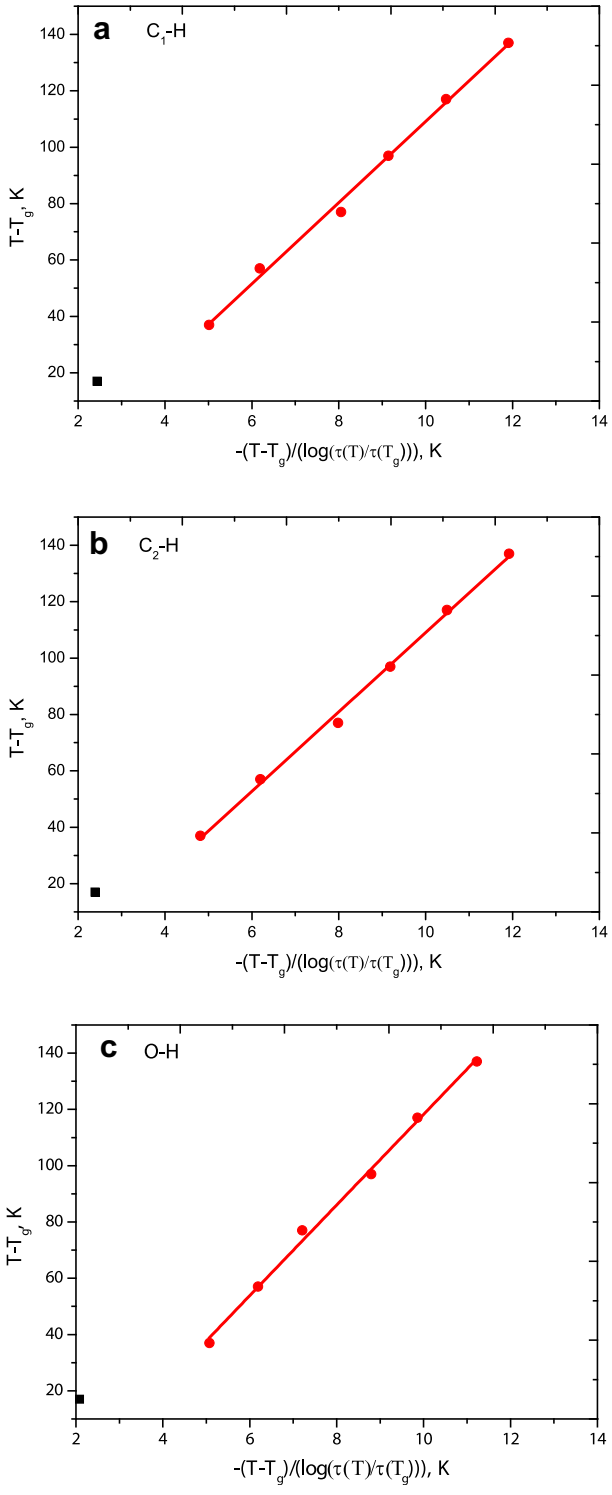

Fig. 12. WLF fit of C1–H bond vector (a) and C2–O (b) bond vector and O–H bond vector (c) on the PVA chain.

the angle acceptor–donor–hydrogen is less than 30°. Several different definitions have been used for HBs [16,17,22,28,29], which are believed not to significantly affect the reported general tendency.

The total HB number per hydroxyl group is plotted as function of temperature, as shown in Fig. 7(a). It can be seen that this value at each temperature is just a bit bigger than the coordination number of water molecules to oxygen atoms of PVA, which indicates that besides between hydroxyl groups and water molecules HBs also form between hydroxyl groups on PVA and between H_2O and H_2O. Furthermore, this value monotonously decreases with increasing temperature, which almost approaches straight line at both temperature regions. An abrupt change in the slope of the straight lines can be obviously seen, which marks the occurrence of glass transition as for the specific volume and diffusion coefficient. This phenomenon confirms that HB interactions in the whole system play a key role in glass transition. When the same analysis procedure is carried out separately on the three pairs, PVA–PVA, PVA–H_2O, and H_2O–H_2O, no similar phenomenon turns up as shown in Fig. 7(b), which suggests that the properties of the whole system (such as T_g) depend on not only the HB interactions between PVA and H_2O (PVA–H_2O) but also on those between PVA and PVA (PVA–PVA) and those between H_2O and H_2O (H_2O–H_2O).

3.4. Local dynamics of PVA

In this part, the local dynamics of PVA would be discussed in terms of Williams–Landel–Ferry (WLF) equation, which is often used to explain the glass transition phenomenon [51].

The second term of the Legendre polynomial is computed for various normalized bond vector autocorrelation functions (VACFs)$\langle u(t)\cdot u(0)\rangle$:

$$P_2(t) = \frac{3}{2}\cdot\left\langle (u(t)\cdot u(0))^2\right\rangle - \frac{1}{2} \tag{10}$$

The decorrelations of the bond vectors containing either non-hydrogen or hydrogen atoms at the temperatures above T_g are shown in Figs. 8–10, where the arrows point at the direction the temperature enhances. It can be seen that, at the higher temperatures, the decrease in the vector orientation is more rapid, indicating that the chain segments are more mobile, as expected. In order to extrapolate the simulation time to the practical time scale the glass transition occurs, these functions are required to be fitted by a defined mathematic function. Towards this aim, the Kolsrauch–Williams–Watt function is employed:

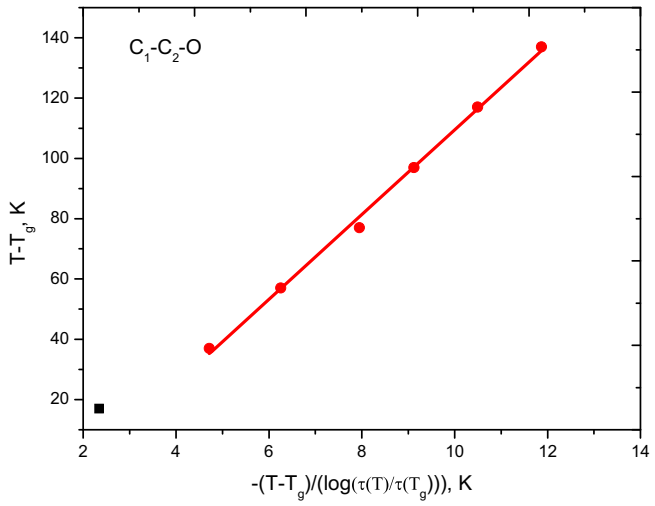

Fig. 13. WLF fit of C1–C2–O bond vector on the PVA chain.

Table 3
Parameters used for the fits of WLF curves for various orientation functions.

Orientation type	C_1^g	C_2^g, K	ΔH_{ap}^{WLF}, kJ/mol
C1–H	14.4	34.8	9.6
C2–H	14.1	31.7	8.6
O–H	16.1	42.8	13.2
C1–C2	13.9	32.7	8.7
C2–O	13.8	28.9	7.6
C1–C2–O	14.1	31.1	8.4

$$\phi(t) = \exp\left[-(t/\tau)^{\beta}\right] \tag{11}$$

in which τ is the average relaxation time, β represents the deviation from a simple exponential decay: $0<\beta<1$. Except at the lowest temperature 300 K due to the statistic error, the fits are found practically very well at the other temperatures above T_g.

By integrating the fitted functions with t from 0 to ∞, the correlation time can be obtained, which gives the following form:

$$\tau_c = \frac{\tau}{\beta}\Gamma\left(\frac{1}{\beta}\right) \tag{12}$$

where Γ represents Gamma function with a single parameter. The correlation times are reported in Table 2 for various bond vectors at various temperatures. These values are several to hundred times the average relaxation time, as a result of many cooperative transitions of neighboring dihedrals [29]. These correlation times can also quantify the motions of chain segments.

According to the Williams–Landel–Ferry (WLF) equation, or the equivalent Vogel–Fulcher–Tammann (VFT) equation [51], the following relation is deduced:

$$T - T_g = C_1^g\left(-\frac{T-T_g}{\log(\tau(T)/\tau(T_g))}\right) - C_2^g \tag{13}$$

in which the correlation time at T_g, $\tau(T_g)$ is set as 100 s, C_1^g and C_2^g are two parameters, which can be accessed by fitting the straight line to the above relation. The corresponding results are shown in Figs. 11–13. Compared to the original WLF equation [51], the apparent activation energies can be evaluated according to the following relation:

$$\Delta H_{ap}^{WLF} = \ln(10)RC_1^gC_2^g \tag{14}$$

Once again, the data at the 300 K is not included in the fitting procedure due to the biggest statistic error at this temperature. The correlation coefficients are all over 0.995, meaning a good fit above T_g. The so-obtained C_1^g and C_2^g are shown in Table 3 together with ΔH_{ap}^{WLF}. No corresponding experimental data are available for comparison. However, these data are all dropped into the same order of general polymers [51].

4. Conclusion

In this work, extensive MD simulations have been carried out on the aqueous PVA containing about 21 wt% H_2O over a wide temperature range across T_g. Many simulated results, including T_g, LCTE, D, RDF, and VACF, are in good agreements with the available data in the literature, which validate the employed molecular model and force field. Besides, for the first time, a break is found for the $\ln(D)$–$1/T$ plot of water in the PVA matrix around T_g, and the orientation behavior of various bond vectors on the PVA chains at above T_g can be well fitted by the WLF equations. These results strongly suggest that dynamics of both PVA and H_2O are responsible for the glass transition of the binary system. Furthermore, this can be explained by the HB interactions: around T_g, total HB number presents an abrupt intersection.

In a word, this work demonstrates the cooperative behavior of PVA and H_2O which is responsible for the glass transition of the whole binary system. While the MD simulation can reproduce many experimental characterizations about structure and properties of PVA–H_2O, the insoluble behavior at lower temperatures is not observed in this work. It is partly due to the slow relaxation at lower temperatures. Since MD simulations have the internal limitations, we cannot expect that MD simulations can reproduce all the realities. Moreover, the reported relations are built for the middle water content. For the lower and higher water contents, whether the same relations also apply remains to be discovered in the future.

Acknowledgements

The author is indebted to the Molecular Simulation Center of Hunan Province (situated Hunan University) and Henan University of Urban Construction which provided the commercial software (Materials Studio-4.0) and hardware, respectively, for completing this work. My colleague Mrs. Yijiang Liu is greatly appreciated for aiding me to revise the manuscript. The author also wishes to acknowledge his wife Mrs. Wanhua Yang for the sustained encouragements and supports, and their daughter Jing Wu for bringing many joys to the family, who motivates some good ideas in his mind.

References

[1] Ao ZM, Zheng WT, Jiang Q. Polymer 2008;49:3578–81.
[2] Delpouve N, Saiter A, Mano JF, Dargent E. Polymer 2008;49:3130–5.
[3] Encinar M, Guzman E, Prolongo MG, Rubio RG, Sandoval C, Gonzalez-Nilo F, et al. Polymer 2008;49:5650–8.
[4] Svoboda R, Pustkova P, Malek J. Polymer 2008;49:3176–85.
[5] Akabori K-I, Atarashi H, Ozawa M, Kondo T, Nagamura T, Tanaka K. Polymer 2009;50:4868–75.
[6] Khan AN, Hong P-D, Chuang W-T, Shih K-S. Polymer 2009;50:6287–96.
[7] Magon A, Pyda M. Polymer 2009;50:3967–73.
[8] Smith KE, Parks SS, Hyjek MA, Downey SE, Gall K. Polymer 2009;50:5112–23.
[9] Erber M, Khalyavina A, Eichhorn K-J, Voit BI. Polymer 2010;51:129–35.
[10] Lai C, Ayyer R, Hiltner A, Baer E. Polymer 2010;51:1820–9.
[11] Lin C-T, Kuo S-W, Huang C-F, Chang F-C. Polymer; 2010:883–9.
[12] Liu T, Siegel RW, Ozisik R. Polymer 2010;51:540–6.
[13] Navarro A, Fernandez-Liencres MP, Pena-Ruiz T, Granadino-Roldan JM, Fernandez-Gomez M, Domınguez-Espinosa G, et al. Polymer 2009;50:317–27.
[14] Wu R, Kong B, Yang X. Polymer 2009;50:3396–402.
[15] Yani Y, Lamm MH. Polymer 2009;50:1324–32.
[16] Tamai Y, Tanaka H, Nakanishi K. Mol Simul 1996;16:359–74.
[17] Tamai Y, Tanaka H, Nakanishi K. Macromolecules 1996;29(21):6750–60.
[18] Tamai Y, Tanaka H, Nakanishi K. Macromolecules 1996;29(21):6761–9.
[19] Tamai Y, Tanaka H. Chem Phys Lett 1998;285:127–32.
[20] Tamai Y, Tanaka H. Fluid Phase Equilib 1998;144:441–8.
[21] Tamai Y, Tanaka H. Phys Rev E 1999;59(5):5647.
[22] Tamai Y, Tanaka H. Mol Simul 1999;21:283–301.
[23] Muller-Plathe F, van Gunsteren WF. Polymer 1997;38(9):2259–68.
[24] Muller-Plathe F. Macromolecules 1998;31(19):6721–3.
[25] Muller-Plathe F. J Membr Sci 1998;141:147–54.
[26] Karlsson GE, Johansson TS, Gedde UW, Hedenqvist MS. J Macromol Sci Part B 2002;42(2):185–206.
[27] Karlsson GE, Gedde UW, Hedenqvist MS. Polymer 2004;45:3893–900.
[28] Chiessi E, Cavalieri F, Paradossi G. J Phys Chem B 2005;109:8091–6.
[29] Chiessi E, Cavalieri F, Paradossi G. J Phys Chem B 2007;111:2820–7.
[30] Bermejo JS, Ugarte CM. J Chem Phys 2008;129:154907.
[31] Hodge RM, Bastow TJ, Edward GH, Simon GP, Hill AJ. Macromolecules 1996;29:8137–43.
[32] Jorgensen WL, Maxwell DS, Tirado-Rives J. J Am Chem Soc 1996;118: 11225–36.
[33] Jorgensen WL, Chandrasekhar J, Madura JD, Impey RW, Klein ML. J Chem Phys 1983;79:926.
[34] Ferrando N, Lachet V, Teuler J-M, Boutin A. J Phys Chem B 2009;113:5985–95.
[35] Materials Studio4.0, Visualizer, amorphous cell, discover. San Diego, CA: Accelry Inc.; 2005.
[36] Theodorou DN, Suter UW. Macromolecules 1985;18:1467–78.
[37] Sun H. J Phys Chem B 1998;102:7338–64.
[38] van der Spoel D, Lindahl E, Hess B, Groenhof G, Mark AE, Berendsen HJC. J Comput Chem 2005;26(16):1701–18.
[39] Hess B, Kutzner C, van der Spoel D, Lindahl E. J Chem Theory Comput 2008;4(3):435–47.
[40] Berendsen HJC, Postma JPM, van Gunsteren WF, DiNola A, Haak JR. J Chem Phys 1984;81:3684.
[41] Parrinello M, Rahman A. J Appl Phys 1981;52(12):7182.
[42] Nosé S. J Chem Phys 1984;81:511.
[43] Hoover WG. Phys Rev A 1985;31:1695–7.
[44] Mark JE. Polymer data handbook. Oxford: Oxford University Press; 1999.
[45] Muller-Plathe F. J Chem Phys 1998;108(19):8252.
[46] Lin YC, Chen X. Chem Phys Lett 2005;412:322–6.
[47] Chen Z, Gu Q, Zou H, Zhao T, Wang H. J Polym Sci Part B 2007;45:884–91.
[48] van der Vegt NFA. Macromolecules 2000;33:3153–60.
[49] Mozaffari F, Eslami H, Moghadasi J. Polymer 2010;51:300–7.
[50] Satokawa Y, Shikata T. Macromolecules 2008;41(8):2908–13.
[51] Soldera A, Grohens Y. Macromolecules 2002;35:722–6.